Article

Catalysis of the Cleavage of Uridine 3‘-2,2,2-Trichloroethylphosphate by a Designed Helix–Loop–Helix Motif Peptide

Jesus Razkin, Helena Nilsson, and Lars Baltzer

J. Am. Chem. Soc., **2007**, 129 (47), 14752-14758 • DOI: 10.1021/ja075478i

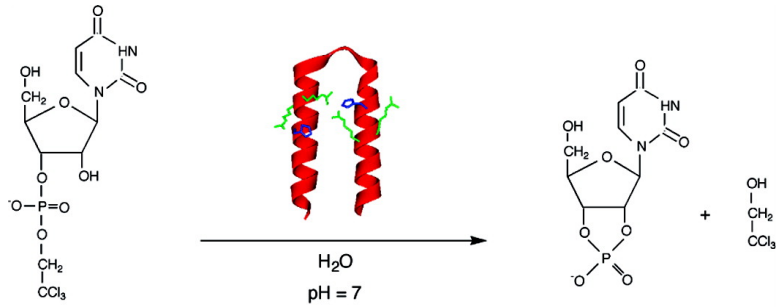

More About This Article

Additional resources and features associated with this article are available within the HTML version:

- Supporting Information
- Links to the 3 articles that cite this article, as of the time of this article download
- Access to high resolution figures
- Links to articles and content related to this article
- Copyright permission to reproduce figures and/or text from this article

View the Full Text HTML

J|A|C|S
ARTICLES
Published on Web 11/07/2007

Catalysis of the Cleavage of Uridine 3′-2,2,2-Trichloroethylphosphate by a Designed Helix−Loop−Helix Motif Peptide

Jesus Razkin,*,† Helena Nilsson,‡ and Lars Baltzer*,§

Contribution from Department of Applied Chemistry, Public University of Navarra, 31006 Pamplona, Navarra, Spain, Department of Organic Chemistry, IFM, Linköping University, SE-58183 Linköping, Sweden, and Department of Biochemistry and Organic Chemistry, Uppsala University, Box 576, SE-75123 Uppsala, Sweden

Received July 23, 2007; E-mail: jrazk@unavarra.es; Lars.Baltzer@biorg.uu.se

Abstract: A 42-residue peptide that folds into a helix−loop−helix motif and dimerizes to form a four-helix bundle has been designed to catalyze the hydrolysis of phosphodiesters. The active site on the surface of the folded catalyst is composed of two histidine and four arginine residues, with the capacity to provide general acid, general base, and/or nucleophilic catalysis as well as transition state stabilization. Uridine 3′-2,2,2 trichloroethylphosphate (**2**) is a mimic of RNA with a leaving group pK_a of 12.3. Its hydrolysis is energetically less favorable than that of commonly used model substrates with *p*-nitrophenyl leaving groups and therefore a more realistic model for the design of catalysts capable of cleaving RNA. The second-order rate constant for the hydrolysis of **2** at pH 7.0 by the polypeptide catalyst was 418×10^{-6} M^{-1} s^{-1}, and that of the imidazole catalyzed reaction was 1.66×10^{-6} M^{-1} s^{-1}. The pH dependence suggested that catalysis is due to the unprotonated form of a residue with a pK_a of around 5.3, and the observed kinetic solvent isotope effect of 1.9 showed that there is significant hydrogen bonding in the transition state, consistent with general acid−base catalysis. The rate constant ratio k_2(Pep)/k_2(Im) of 252 is probably due to a combination of nucleophilic and general acid−base catalysis, as well as transition state stabilization. Substrate binding was weak since no sign of saturation kinetics was observed for substrate concentrations in the range from 5 to 40 mM. The results provide a platform for the further development of catalysts for RNA cleavage with a potential role in the development of drugs.

Introduction

An understanding of the fundamental principles of enzyme catalysis will arise from a detailed study of the relation between structure, dynamics, molecular recognition, interactions, and reactivity in proteins. In that context, a key complementary role is played by the *de novo* designed proteins[1−2] where natural and non-natural amino acids can be organized in a variety of differently planned forms and geometries, accommodating many potential reactive sites that could catalyze important chemical reactions, provided that the proper tertiary structure could be precisely predicted and successfully reached. We reported previously on the reactivity of functionalized helix−loop−helix dimers[3] and have now embarked on a search for new and efficient catalysts for the hydrolysis of polynucleotides using a four-helix bundle polypeptide scaffold in which residue types and geometries can be systematically varied.

Phosphodiester bonds form the backbone of DNA and RNA biopolymers, and phosphorylation reactions are key events in transmembrane signaling, in cellular energy regulation, and in multiple biosynthesis pathways.[4] And in the era of proteomics RNA is a key target in drug development due to its role in the expression of proteins *in vivo*. Sense and antisense or siRNA strategies have become important concepts in drug development, but it is conceivable that simply binding to RNA is not sufficient for efficient combat of disease. Chemically the cleavage of RNA represents a bigger challenge but also, if successful, a better defined solution to the problem of controlling protein expression levels. In addition to providing clues about how to modulate RNA activity, the design of catalysts for RNA hydrolysis

† Public University of Navarra.
‡ Linköping University.
§ Uppsala University.

(1) (a) Mutter, M.; Vuilleumier, S. *Angew. Chem., Int. Ed. Engl.* **1989**, *28*, 535−554. (b) Struthers, M. D.; Cheng, R. P.; Imperiali, B. *Science* **1996**, *271*, 342−345. (c) Dahiyat, B. I.; Mayo, S. L. *Science* **1997**, *278*, 82−87. (d) Kohn, W. D.; Hodges, R. S. *Trends Biotechnol. TIBTECH* **1998**, *16*, 379−389. (e) Micklatcher, C.; Chmielewski, J. *Curr. Opin. Chem. Biol.* **1999**, *3*, 724−729. (f) Lacroix, E.; Kortemme, T.; Lopez de la Paz, M.; Serrano, L. *Curr. Opin. Struct. Biol.* **1999**, *9*, 487−493. (g) Hill, B. R.; Raleigh, D. P.; Lombardi, A.; DeGrado, W. F. *Acc. Chem. Res.* **2000**, *33*, 745−754. (h) Baltzer, L.; Nilsson, H.; Nilsson, J. *Chem. Rev.* **2001**, *101*, 3153−3163. (i) Calhoun, J. R.; Kono, H.; Lahr, S.; Wang, W.; DeGrado, W. F.; Saven, J. G. *J. Mol. Biol.* **2003**, *334*, 1101−1115. (j) Kaplan, J.; DeGrado, W. F. *Proc. Natl. Acad. Sci. U.S.A.* **2004**, *101*, 11566−11570. (k) Calhoun, J. R.; Nastri, F.; Maglio, O.; Pavone, V.; Lombardi, A.; DeGrado, W. F. *Biopolymers* **2005**, *80*, 264−278.
(2) (a) Bryson, J. W.; Betz, S. F.; Lu, H. S.; Suich, D. J.; Zhou, H. X.; O'Neill, K. T.; DeGrado, W. F. *Science* **1995**, *270*, 935−941. (b) Betz, S. F.; DeGrado, W. F. *Biochemistry* **1996**, *35*, 6955−6962.
(3) (a) Broo, K.; Brive, L.; Lundh, A.-C.; Ahlberg, P.; Baltzer, L. *J. Am. Chem. Soc.* **1996**, *118*, 8172−8173. (b) Baltzer, L.; Lundh, A.-C.; Broo, K.; Olofsson, S.; Ahlberg, P. *J. Chem. Soc., Perkin Trans. 2* **1996**, 1671−1676. (c) Broo, K.; Allert, M.; Andersson, L.; Erlandsson, P.; Stenhagen, G.; Wigström, J.; Ahlberg, P.; Baltzer, L. *J. Chem. Soc., Perkin Trans. 2* **1997**, 397−398.
(4) Fersht, A. In *Enzyme Structure and Mechanism*; W. H. Freeman and Co.: New York, 1985; pp 259 and 491.

10.1021/ja075478i CCC: $37.00

promises insights into fundamental aspects of enzyme catalysis. Phosphodiester linkages are extremely stable and resistant to hydrolysis[5] so that enzymes that have evolved to catalyze their hydrolysis are among the most efficient ones known, with rate enhancements of 18 orders of magnitude or more, stemming from a combination of general acid and general base catalysis, transition stabilization, and proximity effects. While nature has evolved a catalytic machinery based on the reactivity of histidine residues, this is not necessarily the only arrangement capable of large rate enhancements, though the design of new man-made artificial nucleases to match the high efficiency of natural ones constitutes a formidable but very interesting challenge.[6]

Many artificial nucleases have already been described.[7] So far, most of the effort has been focused on metallonucleases, since many natural enzymes that cleave phosphodiester bonds incorporate two or three metal ions in their active site.[8] These enzymes take advantage of the Lewis acid properties of metals for biochemical reactions, their affinity for basic nitrogen and oxygen donor ligands, the capacity to support large aromatic architectures capable of π interactions with the nucleic acid building blocks, the ability to directly hydrolyze phosphodiester linkages, and the possibility of promoting redox chemistry or generate reactive oxygen-derived species.[9] But the time-dependent exchange reactions of metal ions[7a] and the slow penetration to cells of metal ion chelates tethered to oligonucleotide based drugs[7a] together with the need of a more efficient binding to the target nucleic acid,[7b,c] often too dependent on direct coordination to the metal center, are significant problems still to be solved.

Among metal-free catalysts, remarkable results showing both cleavage activity and sequence recognition have been obtained using diethylenetriamine-ODN (oligodeoxyribonucleotides),[10] imidazole containing ODNs,[11] peptides conjugated to ODNs,[12] methanephosphonate ODNs with diimidazole or an imidazole/amino cleaving agent,[13] a PNA (peptide nucleic acid) conjugate of neamine,[14] and a PNA linked diethylenetriamine moiety.[15]

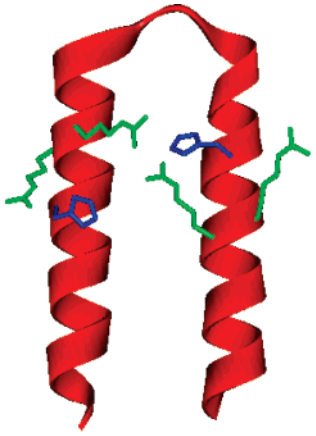

Ac-N-A-A-D-Nle-E-A-A-I-K-H[11]-L-A-R[14]-R[15]-Nle-A-A-K-
G-P-V-D-
H_2N-G-A-R-A-F-A-E-F-R[34]-R[33]-A-L-H[30]-E-A-Nle-Q-A-A-

Figure 1. Modeled structure of the helix−loop−helix motif and amino acid sequence of HNI. The one letter code for the amino acids is used (A is alanine, D is aspartic acid, E is glutamic acid, F is phenylalanine, G is glycine, H is histidine, I is isoleucine, K is lysine, L is leucine, N is asparagine, P is proline, Q is glutamine, R is arginine, V is valine, and Nle is norleucine). The C-terminal is amidated, and the N-terminal is acetylated. Only the side chains of the residues designed for the catalytic site are shown, and although the active peptide is in the dimer form, only the monomer is shown for clarity of presentation.

Recently, a very promising result[16] from Göbel's group has demonstrated that tris(2-aminobenzimidazoles) attached to DNA oligonucleotides act as very efficient nucleases, showing substrate and site selectivity as well as saturation kinetics, thus proving that they could compete with the metal-dependent artificial nucleases.

We have found (unpublished results) that a catalytic site containing four Arg and two His residues on the surface of a helix−loop−helix motif, with two Arg and one His in each helix (Figure 1), is optimal in the reaction of the activated substrate 2-hydroxypropyl *p*-nitrophenylphosphate, HPNP (**1**) (Chart 1). While the study of activated substrates serve as good "early stage" model systems, the catalysis of, e.g., *p*-nitrophenyl esters

(5) (a) Kumamoto, J.; Cox, J. R., Jr.; Westheimer, F. H. *J. Am. Chem. Soc.* **1956**, *78*, 4858−4860. (b) Bunton, C. A.; Mhala, M. M.; Oldham, K. G.; Vernon, C. A. *J. Chem. Soc.* **1960**, 3293−3301. (c) Kirby, A. J.; Younas, M. *J. Chem. Soc. B* **1970**, 510−513. (d) Radzicka, A.; Wolfenden, R. *Science* **1995**, *267*, 90−93. (e) Wolfenden, R.; Ridgway, C.; Young, G. *J. Am. Chem. Soc.* **1998**, *120*, 833−834. (f) Takeda, N.; Shibata, M.; Tajima, N.; Hirao, K.; Komiyama, M. *J. Org. Chem.* **2000**, *65*, 4391−4396. (g) Williams, N. H.; Wyman, P. *Chem. Commun.* **2001**, 1268−1269. (h) Schroeder, G. K.; Lad, C.; Wyman, P.; Williams, N. H.; Wolfenden, R. *Proc. Natl. Acad. Sci. U.S.A.* **2006**, *103*, 4052−4055. (i) Wolfenden, R. *Chem. Rev.* **2006**, *106*, 3379−3396.

(6) Kirby, A. J. *Angew. Chem., Int. Ed. Engl.* **1996**, *35*, 707−724.

(7) Reviews: (a) Niittymäki, T.; Lönnberg, H. *Org. Biomol. Chem.* **2006**, *4*, 15−25. (b) Morrow, J. R.; Iranzo, O. *Curr. Opin. Chem. Biol.* **2004**, *8*, 192−200. (c) Cowan, J. A. *Curr. Opin. Chem. Biol.* **2001**, *5*, 634−642. (d) Häner, R. *Chimia* **2001**, *55*, 1035−1037. (e) Komiyama, M.; Sumaoka, J.; Kuzuya, A.; Yamamoto, Y. *Methods Enzymol.* **2001**, *341*, 455−468. (f) Mikkola, S.; Kaukinen, U.; Lönnberg, H. *Cell Biochem. Biophys.* **2001**, *34*, 95−119. (g) Zenkova, M.; Beloglazova, N.; Silnikov, V.; Vlassov, V.; Giege, R. *Methods Enzymol.* **2001**, *341*, 468−490. (h) Kimura, E. *Curr. Opin. Chem. Biol.* **2000**, *4*, 207−213. (i) Trawick, B.; Daniher, A. T.; Bashkin, J. K. *Chem. Rev.* **1998**, *98*, 939−960. (j) Komiyama, M.; Sumaoka, J. *Curr. Opin. Chem. Biol.* **1998**, *2*, 751−757. (k) Häner, R.; Hall, J. *Antisense Nucleic Acid Drug Dev.* **1997**, *7*, 423−430. (l) Komiyama, M. *J. Biochem.* **1995**, *118*, 665−670.

(8) (a) Weston, J. *Chem. Rev.* **2005**, *105*, 2151−2174. (b) Jedrzejas, M. J.; Setlow, P. *Chem. Rev.* **2001**, *101*, 607−618. (c) Cowan, J. A. *Chem. Rev.* **1998**, *98*, 1067−1087. (d) Wilcox, D. E. *Chem. Rev.* **1996**, *96*, 2435−2458. (e) Strater, N.; Lipscomb, W. N.; Klabunde, T.; Krebs, B. *Angew. Chem., Int. Ed. Engl.* **1996**, *35*, 2024−2055.

(9) Boerner, L. J. K.; Zalesky, J. M. *Curr. Opin. Chem. Biol.* **2005**, *9*, 135−144.

(10) (a) Komiyama, M.; Inokava, T.; Yoshinari, K. *Chem. Commun.* **1995**, 77−78. (b) Komiyama, M.; Inokava, T. *J. Biochem.* **1994**, *116*, 719−720. (c) Endo, M.; Azuma, Y.; Saga, Y.; Kuzuya, A.; Kawai, G.; Komiyama, M. *J. Org. Chem.* **1997**, *62*, 846−852.

(11) (a) Vlassov, V.; Abramova, T.; Giege, R.; Silnikov, V. *Antisense Nucleic Acid Drug Dev.* **1997**, *7*, 39−42. (b) Yurchenko, L.; Silnikov, V.; Godovikova, T.; Shishkin, G.; Toulme, J.-J.; Vlassov, V. *Nucleosides Nucleotides* **1997**, *16*, 1721−1725. (c) Beloglazova, N. G.; Silnikov, V. N.; Zenkova, M. A.; Vlassov, V. V. *FEBS Lett.* **2000**, *481*, 277−280. (d) Beloglazova, N. G.; Epanchintsev, A. Y.; Silnikov, V. N.; Zenkova, M. A.; Vlassov, V. V. *Mol. Biol., Engl. Ed.* **2002**, *36*, 581−588. (e) Beloglazova, N. G.; Fabani, M. M.; Zenkova, M. A.; Bichenkova, E. V.; Polushin, N. N.; Silnikov, V. V.; Douglas, K. T.; Vlassov, V. V. *Nucleic Acids Res.* **2004**, *32*, 3887−3897.

(12) (a) Mironova, N. L.; Pyshnyi, D. V.; Ivanova, E. M.; Zenkova, M. A.; Gross, H. J.; Vlassov, V. V. *Nucleic Acids Res.* **2004**, *32*, 1928−1936. (b) Mironova, N. L.; Pyshnyi, D. V.; Ivanova, E. M.; Zarytova, V. F.; Zenkova, M. A.; Gross, H. J.; Vlassov, V. V. *Russ. Chem. Bull.* **2002**, *51*, 1177−1186. (c) Mironova, N. L.; Boutorine, Y. I.; Pyshnyi, D. V.; Ivanova, E. M.; Zenkova, M. A.; Vlassov, V. V. *Nucleosides, Nucleotides Nucleic Acids* **2004**, *23*, 885−890.

(13) (a) Reynolds, M. A.; Beck, T. A.; Say, P. B.; Schwartz, D. A.; Dwyer, B. P.; Daily, W. J.; Vaghefi, M. M.; Metzler, M. D.; Klem, R. E.; Arnold, L. J., Jr. *Nucleic Acids Res.* **1996**, *24*, 760−765. (b) Ushijima, K.; Takaku, H. *Biochim. Biophys. Acta* **1998**, *1379*, 217−223.

(14) Riguet, E.; Tripathi, S.; Chaubey, B.; Desire, J.; Pandey, V. N.; Decout, J.-L. *J. Med. Chem.* **2004**, *47*, 4806−4809.

(15) (a) Verheijen, J. C.; Deiman, B. A. L. M.; Yeheskiely, E.; van der Marel, G. A.; van Boom, J. H. *Angew. Chem., Int. Ed.* **2000**, *39*, 369−372. (b) Petersen, L.; de Koning, M. C.; van Kuik-Romeijn, P.; Weterings, J.; Pol, C. J.; Platenburg, G.; Overhand, M.; van der Marel, G. A.; van Boom, J. H. *Bioconjugate Chem.* **2004**, *15*, 576−582.

(16) (a) Gnaccarini, C.; Peter, S.; Scheffer, U.; Vonhoff, S.; Klussmann, S.; Göbel, M. W. *J. Am. Chem. Soc.* **2006**, *128*, 8063−8067. (b) Scheffer, U.; Strick, A.; Ludwig, V.; Peter, S.; Kalden, E.; Göbel, M. W. *J. Am. Chem. Soc.* **2005**, *127*, 2211−2217.

Chart 1 Structure of the RNA Analogues Used as Substrates: 2-Hydroxypropyl-*p*-nitrophenyl Phosphate (HPNP) (**1**), Uridine 3′-(2,2,2-Trichloroethylphosphate) (**2**), and 2-Hydroxypropyl-2,2,2-trichloroethyl Phosphate (**3**)

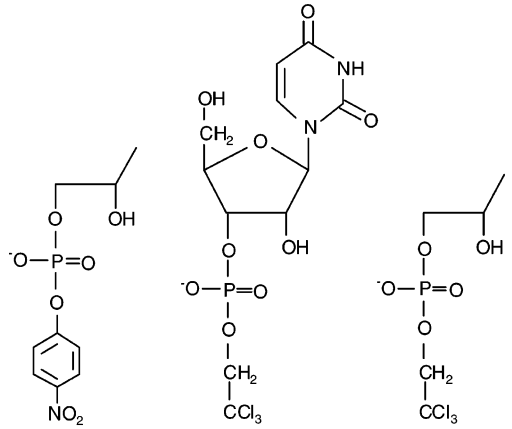

may have little relevance for the engineering of competent catalysts for RNA hydrolysis, since efficient cleavage of aryl esters does not necessarily mean efficient cleavage of RNA.[7a] We report now on the catalysis of hydrolysis of an RNA model substrate, uridine 3′-2,2,2-chloroethyl phosphate (**2**) (Chart 1), in which the leaving group pK_a is 12.3, close to that of a ribose OH and more than 5 pK_a units higher than that of *p*-nitrophenol. While the results reported here address only the catalytic machinery, it should be noted that the specificity problem has already been solved by the design and synthesis of nucleotide mimicking compounds, such as PNA. The catalysts developed in the four-helix bundle scaffold are readily linked to PNA using well-known chemistry.

Results and Discussion

The ultimate objective of the *de novo* catalyst design is to obtain artificial enzymes that catalyze chemical reactions in the same specific and efficient way as native enzymes. We can already obtain very good binding interactions,[17] in binding sites with high affinities comparable to those of natural enzymes: but it is still very difficult to achieve the proper organization of reactive sites to support the desired catalysis levels. We still have a long way to go, especially in our understanding of how to set up the desired chemical reaction mechanisms with designed enzymes. Nevertheless, the high efficiencies obtained in simple model catalysts show that better results could arise from the proper adjustment of those catalytic sites with binding of substrate, intermediate, and transition state. Thus, the rapid broadening of the study field and application scope has attracted the interest and effort of many research groups, showing at the same time that function, rather than only structure, has become the focus in protein engineering and design.[18]

Trying to broaden this knowledge, we have focused on the four-helix bundle motif, a robust and sophisticated peptidic scaffold in which residue types and geometries can be systematically varied. The motif is very useful since it is readily synthesized, can be site-selectively functionalized, ensures water solubility for covalently linked groups, and provides high design−versatility with the possibility of having many different functionalities in a variety of determined geometries. It could have many interesting applications in drug development, biomedicine, proteomics, or biosensing. Now we have explored these folded polypeptides as catalysts for the hydrolysis of simple RNA model phosphate diesters **1**−**3** (Chart 1), with the long-term aim of development of new and efficient ribonucleases.

Catalyst Design. The design of HNI (Figure 1) will not be described in detail (unpublished results). It was based on the sequence of the *de novo* designed template polypeptide SA-42[19] and on the understanding that evolved from extensive studies of structure and dynamics of that parent peptide and of the polypeptides[20−22] derived from the same template.

These 42-residue sequences, and therefore HNI, were designed to fold into two amphiphilic helical segments linked by a four-residue loop, form a hairpin helix−loop−helix motif, and dimerize in an antiparallel mode to form a four-helix bundle.[19] In short, the design is described in terms of the heptad repeat pattern[2a] (a-b-c-d-e-f-g)*n* in which the residues in the *a* and *d* positions form the hydrophobic core, those in the *c* and *g* positions form the exposed surface of the dimer, and the residues in the *b* and *e* positions are at the dimer interface and control dimerization. The amino acid residues were selected based on their propensities for secondary structure formation[23] and their ability to stabilize the helical folded structure by formation of salt bridges and stabilization of the helix dipole moment.[2] The C- and N-terminus were capped by amidation and acylation, respectively. Shape complementary hydrophobic interfaces were obtained using leucine, isoleucine, norleucine, phenylalanine, and valine to create hydrophobic interactions between amphiphilic helices upon folding, thus driving the formation of the helix−loop−helix hairpin and its dimerization.

A detailed analysis of the solution structure of HNI has not been carried out because of its large sequence homology with the parent polypeptides, which were extensively characterized by NMR and CD spectroscopy and analytical ultracentrifugation. We assume based on the similarity with the parent sequences that HNI adopts the same fold. The mean residue ellipticity of a polypeptide at 222 nm, Θ_{222}, is an established probe of helix formation and a good reporter of dimer formation for the sequences mentioned here. All sequences derived from the SA-42 family of peptides show a strong concentration dependence and low helical content in the monomeric state. The CD spectrum of HNI shows the hallmarks of a helical protein,[24] with minima at 208 and 222 nm. The mean residue ellipticity of HNI at 222 nm and 0.5 mM was −20 396 deg cm^2 dmol^{-1}

(17) (a) Cooper, W. J.; Waters, M. L. *Curr. Opin. Chem. Biol.* **2005**, *9*, 627−631. (b) Andersson, T.; Lundquist, M.; Dolphin, G. T.; Enander, K.; Jonsson, B.-H.; Nilsson, J. W.; Baltzer, L. *Chem. Biol.* **2005**, *12*, 1245−1252. (c) Enander, K.; Dolphin, G. T.; Baltzer, L. *J. Am. Chem. Soc.* **2004**, *126*, 4464−4465. (d) Looger, L. L.; Dwyer, M. A.; Smith, J. J.; Hellinga, H. W. *Nature* **2003**, *423*, 185−190.
(18) Baltzer, L.; DeGrado, W. F. *Curr. Opin. Struct. Biol.* **2004**, *14*, 455−457.
(19) (a) Olofsson, S.; Johansson, G.; Baltzer, L. *J. Chem. Soc., Perkin Trans. 2* **1995**, 2047−2056. (b) Olofsson, S.; Baltzer, L. *Folding Des.* **1996**, *1*, 347−356.
(20) Broo, K. S.; Brive, L.; Ahlberg, P.; Baltzer, L. *J. Am. Chem. Soc.* **1997**, *119*, 11362−11372.
(21) Andersson, L. K.; Dolphin, G. T.; Kihlberg, J.; Baltzer, L. *J. Chem. Soc., Perkin Trans. 2* **2000**, 459−464.
(22) Andersson, L. K.; Caspersson, M.; Baltzer, L. *Chem.−Eur. J.* **2002**, *8*, 3687−3697.
(23) (a) Chou, P. Y.; Fasman, G. D. *Biochemistry* **1974**, *13*, 211−222. (b) Chou, P. Y.; Fasman, G. D. *Biochemistry* **1974**, *13*, 222−244. (c) Richardson, J. S.; Richardson, D. C. In *Prediction of Protein Structure and the Principles of Protein Conformation*; Fasman, G. D., Ed.; Plenum Press: New York, 1989; pp 1−88.
(24) Johnson, W. C., Jr. *Proteins* **1990**, *7*, 205−214.

at pH 7.0 and room temperature, which compares well with other sequences. We conclude that HNI folds under those conditions into a helix−loop−helix motif that dimerizes to form a four-helix bundle.

HNI was synthesized by solid-phase peptide synthesis on an Applied Biosystems Pioneer automated peptide synthesizer, using an Fmoc strategy (9-fluorenylmethoxycarbonyl protection group), purified by reversed-phase HPLC, and identified using a Voyager MALDI-TOF mass spectrometer.

Reactivity of HNI. The reactive site for the hydrolysis of phosphate esters was designed based on fundamental principles of organic reactivity. Histidine residues were introduced on the surface of the folded polypeptide, Figure 1, to take advantage of the catalytic potential of its imidazole side chain to provide nucleophilic, general acid, and/or general base catalysis. The protonated and unprotonated forms of the imidazole groups are also capable of binding substrates, intermediates, and transition states since they are good proton donors and acceptors. The flanking arginine residues were introduced to bind the negatively charged phosphate esters and their even more negatively charged transition states and intermediates by electrostatic interactions and hydrogen bonding. An efficient neutralization of those negative charges constitute a necessary requirement in order to achieve any cleaving catalysis.

We find that this reactive site successfully catalyzes the cleavage of the activated phosphate diester HPNP (**1**) (Chart 1) at pH 7.0 and 303 K with a second-order rate constant, k_2, of 7.08×10^{-4} M^{-1} s^{-1}, 621 times bigger than the imidazole catalyzed reaction ($k_2(\mathrm{Im}) = 1.14 \times 10^{-6}$ M^{-1} s^{-1}). HPNP undergoes an intramolecular phosphoryl transfer reaction with release of the *p*-nitrophenol leaving group to obtain the cyclic phosphate as the only detectable product. Due to the low pK_a of *p*-nitrophenol, 7.1, the reaction is fast and readily monitored by visible spectroscopy at 405 nm. Although this activated substrate is extensively used as an RNA early stage model system, unactivated alkyl phosphates would make more convincing model compounds, since efficient catalysis obtained with aryl esters does not necessarily work similarly with real RNA.[7a] This is explained in terms of the rate-limiting step for the intramolecular transesterification of phosphate diesters, which is determined by the formation of the phosphorane intermediate in the case of aryl phosphodiesters while in the case of alkyl phosphates is determined by the breakdown of that intermediate.[25]

Thus, we have studied the HNI polypeptide catalyst with alkyl phosphates **2** and **3** (Chart 1). 2-Hydroxypropyl-2,2,2-chloroethyl phosphate (**3**) is cyclized under the same conditions as those for HPNP, in this case with the release of 2,2,2-chloroethanol, though the 2,2,2-chloroethoxide leaving group has a pK_a of 12.3 and the reaction is considerably slower. Both of these substrates mimic the first step in enzyme catalyzed RNA hydrolysis in which the 2′-OH group attacks the phosphorus atom to form the cyclic intermediate with release of the 5′-OH from the neighboring nucleotide. Both of these substrates are conformationally flexible, and the position of the nucleophilic hydroxyl group relative to the phosphate group is not well defined. In contrast, in uridine 3′-(2,2,2-trichloroethylphosphate) (**2**), the nucleophile is fixed relative to the phosphate group, and although the leaving group here too is 2,2,2-chloroethanol, the reaction is relatively fast. As in the case of HPNP, apart from the released leaving groups, the cyclic phosphates are the only detectable products by NMR or HPLC in the intramolecular phosphoryl transfer reaction of **2** and **3**.

Those substrates constitute a very useful set of nucleic acid simple models showing decreasing reactivity depending on the leaving group, the molecule structure, and rigidity of the −OH group that assists intramolecularly and also presenting different sizes, steric requirements, and hydrophobicities. They are readily prepared (see Experimental Section) by a convenient procedure which allows the introduction of a diverse range of chemical structures with many possible structural, hydrophobic, and electronic features that could be combined around the phosphate moiety with another long range of leaving groups having different reactivity levels. This allows the possibility for a stepwise and gradual refinement, improvement, and redesign of the peptide catalysts for each reactivity level inside each structural family. We chose 2,2,2-trichloroethanol as the leaving group since its pK_a value of 12.3[26] is close to that of a ribose 5′-OH, 14.3,[27] and more than 5 pK_a units higher than the 7.1 pK_a value[28] for *p*-nitrophenol activated models.

Since there is no chromophore in the substrate **3** to allow a convenient spectrophotometric measurement of kinetics, cyclization was followed by NMR spectroscopy (Varian Inova Unity 600 MHz). Initial rates of product formation were calculated from the increase in intensity of the resonance of the methyl group from the propane-1,2-diol cyclic phosphate (doublet at δ 1.28 ppm) as a function of time. Care was taken to optimize the signal-to-noise for reactant and product and to ensure that enough time was allowed for relaxation between pulses. Under conditions of initial rates the ^{13}C satellites of the substrates were used as internal references. Kinetic measurements were carried out at 323 K, using 3 mM of peptide and 30 mM of substrate in 50 mM buffer solutions (HEPES, MES, or NaAc). The corresponding reactions with 100 mM imidazole and those in the absence of any catalyst were carried out in parallel. NaCl was added to the peptide solution and to the uncatalyzed "blank" reaction to keep the ionic strength constant in all experiments.

In the case of uridine 3′-(2,2,2-trichloroethylphosphate) (**2**), substrate and cyclization product have the same absorption wavelength so rate constants were determined by HPLC, and initial rates of substrate degradation or product formation were calculated from the integrated areas of the corresponding resolved peaks using an internal standard for calibration of concentrations. The experiments were run at 313 K, using 1 mM peptide and 2 mM substrate in 50 mM buffer solutions (HEPES, MES, or NaAc). Again, imidazole, 50 mM, and an uncatalyzed blank experiment were used as reference reactions, and NaCl was added to keep the ionic strength constant between experiments. As an internal standard 1 mM sodium 3-nitrobenzenesulfonate was used in all cases.

(25) Lönnberg, H.; Strömberg, R.; Williams, A. *Org. Biomol. Chem.* **2004**, *2*, 2165−2167.

(26) Ballinger, P.; Long, F. A. *J. Am. Chem. Soc.* **1960**, *82*, 795−800.

(27) An estimate from the method of Takahashi et al. using the pK_a of the corresponding COOH group of the ribouronic acid (Wu et al.). (a) Takahashi, S.; Cohen, L. A.; Miller, H. K.; Peake, E. G. *J. Org. Chem.* **1971**, *36*, 1205−1209. (b) Wu, J.; Serianni, A. S. *Carbohydr. Res.* **1991**, *211*, 207−217.

(28) (a) Kirby, A. J.; Varvoglis, A. G. *J. Am. Chem. Soc.* **1967**, *89*, 415−423. (b) Bunton, C. A.; Fendler, E. J.; Humeres, E.; Yang, K.-U. *J. Org. Chem.* **1967**, *32*, 2806−2811. (c) Colthurst, M. J.; Nanni, M.; Williams, A. *J. Chem. Soc., Perkin Trans. 2* **1996**, 2285−2291.

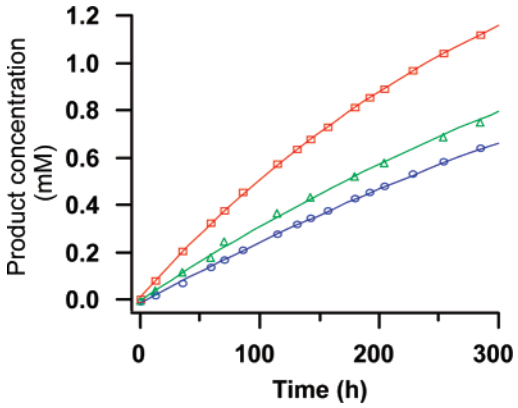

Figure 2. Initial kinetic profile for the cleavage of uridine 3′-(2,2,2-trichloroethylphosphate) (**2**) at pH 7.0 and 313 K by 1 mM peptide (red line/squares) or by 50 mM imidazole (green line/triangles), together with the blank experiment (blue line/circles). Substrate concentrations were 2 mM in 50 mM buffer solution (HEPES), and reactions were followed by HPLC.

Table 1. Initial Rates,[a] Second-Order Rate Constants,[b] and Rate Enhancements for the HNI and Imidazole Catalyzed Cleavage of Substrates **2** and **3** at pH 7.0

		substrate **2**[c]	substrate **3**[d]
imidazole	v_{obs}	0.86×10^{-9}	0.076×10^{-9}
	k_2	1.66×10^{-6}	0.3×10^{-8}
HNI peptide	v_{obs}	1.53×10^{-9}	0.12×10^{-9}
	k_2	418×10^{-6}	59×10^{-8}
rate enhancement k_2(Pep)/k_2(Im)		252	197

[a] v_{obs} obtained under initial rate conditions, data in M s^{-1}. [b] k_2 data in M^{-1} s^{-1}. [c] Conditions: 313 K, 2 mM of substrate in 50 mM buffer solutions (HEPES), 1 mM of peptide, and 50 mM of imidazole. [d] Conditions: 323 K, 30 mM of substrate in 50 mM buffer solutions (HEPES), 3 mM of peptide, and 100 mM of imidazole.

The rate constants were calculated from the slopes of the linear plots of pseudo-first-order kinetics obtained under initial rate conditions (Figure 2). After subtraction of background reaction rates, the slopes of the plot of concentration versus time were divided by the substrate and peptide concentrations to give the second-order rate constant, k_2, an approach that is valid for reactions that do not follow saturation kinetics.

The second-order rate constants for the HNI catalyzed cleavage of **2** and **3** are presented in Table 1, together with those of the imidazole catalyzed reactions, which are used as the reference for comparison since the reactive site of HNI contains His residues. The rate constants are directly comparable, and the efficiency of the designed catalyst can be deduced from the rate constant ratio, k_2(Pep)/k_2(Im). In the case of substrate **3** the ratio is almost a factor of 200, whereas in the case of substrate **2** it is a factor of 252. The catalysis obtained with the peptide, with more than 2 orders of magnitude in rate enhancement compared to imidazole, constitutes a very interesting result in terms of future potential.

The pH dependence of the rate constant ratios is also shown, in Table 2 for substrate **2** and in Table 3 for substrate **3**. An increase in catalysis is observed with increasing pH. At pH 8.0, the imidazole and blank (background) experiments for substrate **2** have the same rate.

Previous studies from Lonnberg's group[29] have shown that the 1-[(2*S*)-2,3-dihydroxypropyl]cytosine derivative, the acyclic analogue of 3′,5′-CpA dinucleoside, is cleaved in aqueous alkali

Table 2. Second-Order Rate Constants and Rate Enhancements for the HNI and Imidazole Catalyzed Cleavage[a] of Substrate **2** at Different pH Values

	k_2 (M^{-1} s^{-1})		rate enhancement
pH	imidazole	HNI	k_2(Pep)/k_2(Im)
4.3	0.14×10^{-6}	21×10^{-6}	150
5	0.31×10^{-6}	47×10^{-6}	152
5.6	0.53×10^{-6}	86×10^{-6}	162
6	0.69×10^{-6}	90×10^{-6}	130
7	1.66×10^{-6}	418×10^{-6}	252
8	0	1944×10^{-6}	*b*

[a] Conditions: 313 K, 2 mM of substrate in 50 mM buffer solutions, 1 mM of peptide, and 50 mM of imidazole. [b] At pH = 8, the imidazol and blank (background) experiments have the same rate.

Table 3. Second-Order Rate Constants and Rate Enhancements for the HNI and Imidazole Catalyzed Cleavage[a] of Substrate **3** at Different pH Values

	k_2 (M^{-1} s^{-1})		rate enhancement
pH	imidazole	HNI	k_2(Pep)/k_2(Im)
5	0.5×10^{-8}	48.9×10^{-8}	98
6	0.43×10^{-8}	52.2×10^{-8}	121
7	0.3×10^{-8}	59×10^{-8}	197

[a] Conditions: 323 K, 30 mM of substrate in 50 mM buffer solutions, 3 mM of peptide, and 100 mM of imidazole.

500 times as fast as CpA. In our case (Table 1) uridine 3′-(2,2,2-trichloroethylphosphate) (**2**) is hydrolyzed by HNI 708 times faster than the acyclic analogue 2-hydroxypropyl-2,2,2-trichloroethylphosphate (**3**) at pH 7.0, k_2(**2**)/k_2(**3**) = 708. As expected from structural differences, and apart from the influence of the fixed position of the hydroxyl group relative to the phosphate in substrate **2**, the result could be explained as a consequence of hydrophobic peptide−substrate interactions. Those interactions, very favorable to substrate **2**, account for higher binding energies than electrostatic ones, which should be similar in both substrates.

In order to determine if the substrate binds to the catalyst strongly enough as to produce saturation kinetics, catalysis of the reaction of **2** by HNI was studied as a function of substrate concentration in the range from 5 to 40 mM, but no evidence for the formation of a peptide−substrate complex was observed (see Supporting Information), since the reaction does not follow saturation kinetics in this concentration range.

Reaction Mechanism. Since these results should not be regarded as a simple bimolecular reaction catalyzed by solvent-exposed His residues, the pH profile of the reaction has been investigated to better understand the efficiency of the catalyst. The pH dependence of the second-order rate constant of the cleavage of **2** is shown in Figure 3. The logarithm of the second-order rate constant increases with pH as expected from a reaction in which catalysis depends on a residue in its unprotonated form. The shape suggests a plateau approximately between pH 5 and 6, after which the rate constant again increases at a pH above 6.5. It is possible to draw a straight line through most of the points although the error limits in the interval between pH 5 and 6 would be considerable, but the line does not have a slope of 1, but only slightly more than 0.5, and is thus incompatible with any simple kinetic model for the catalyzed reaction. A

(29) Oivanen, M.; Mikhailov, S. N.; Florentiev, V. L.; Vihanto, P.; Lönnberg, H. *Acta Chem. Scand.* **1993**, *47*, 622−625.

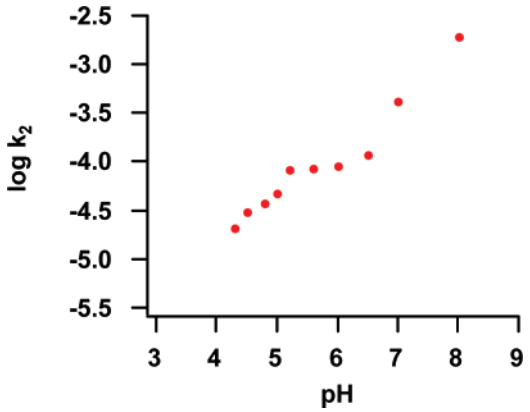

Figure 3. Logarithm of the second-order rate constant k_2 versus pH for the HNI catalyzed cleavage of uridine 3′-(2,2,2-trichloroethylphosphate) (**2**) at 313 K. The kinetics were run with 1 mM peptide and 2 mM substrate concentrations in 50 mM buffers solutions (HEPES, MES, or NaAc) and followed by HPLC.

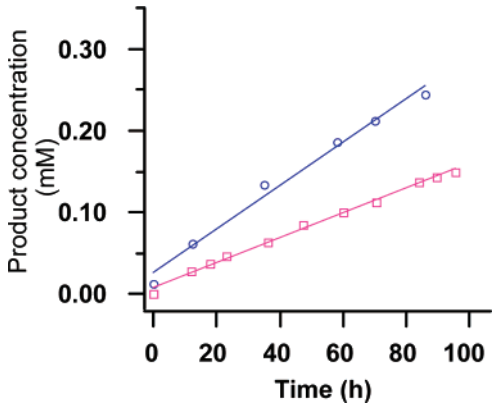

Figure 4. Initial rates for the cleavage of uridine 3′-(2,2,2-trichloroethylphosphate) (**2**) in H_2O (blue line/circles) or in D_2O (pink line/squares) at pH 7.0 and 313 K. The experiments were run using a 1 mM peptide and 2 mM substrate concentrations in 50 mM buffer solution (HEPES) and followed by HPLC. The observed kinetic solvent isotope effect, k_{H_2O}/k_{D_2O}, is 1.9.

plateau in the interval between pH 5 and 6 can be interpreted in terms of the pK_a of a catalytic residue. Our estimate (0.3 log units below the plateau) is close to 5.5, a typical value for His residues. We interpret the pH dependence of the HNI catalyzed reaction of **2** as being due to an unprotonated residue with a pK_a of 5.5. The reason for the observed increase in catalytic activity by HNI above pH 6 is not clear but can simply be the base-catalyzed reaction corresponding to the Im catalyzed parent.

The HNI catalyzed reaction of **3** is independent of pH in the interval between pH 5 and pH 7 but too slow to measure at lower pH values. The mechanistic interpretation is inconclusive, but here also the results are consistent with a mechanism in which catalysis depends on the unprotonated form of a residue with a pK_a in the region expected for His.

Further mechanistic information was obtained from the determination of the kinetic solvent isotope effect at pH 7.0. The second-order rate constants were measured in H_2O and in D_2O solution at pH 7.0 assuming that the solvent isotope effects on the dissociation constants and the pH electrode potentials cancel out. The reaction at a pH* value in D_2O can be compared to the reaction at the same pH value in H_2O since the usual addition of 0.4 pH units to the glass electrode reading on the pH meter is compensated by the equilibrium isotope effect on dissociation constants[30] and the isotopic fractionation of the imidazolium ion can be neglected.[31] The kinetic solvent isotope effect was determined for the HNI catalyzed reactions of **2** and **3**. In the case of **2** the rate constant ratio k_{H_2O}/k_{D_2O} was 1.9 (Figure 4) showing that a proton is in-flight in the transition state, a conclusion usually interpreted[32,30] in terms of general acid−base catalysis. The HNI catalyzed reaction of **3** exhibited a rate constant ratio k_{H_2O}/k_{D_2O} of 1.0, a value that is compatible with a mechanism where there is no hydrogen bond difference between ground and transition states (or compensating hydrogen bonding in ground and transition states). Without supporting evidence we have no grounds for assuming compensating effects, and we conclude that general acid and/or general base catalysis does not occur in the rate-determining step for the reaction of **3**.

Further development of the HNI peptide catalyst will be directed toward larger rate enhancements and improved substrate binding. Studies are underway with the introduction of residues that could better bind the substrates and the transition states, which at the same time would lead to a more efficient catalysis.

Conclusions

The results show that a four-helix bundle catalyst engineered by rational design can successfully catalyze the hydrolysis and cyclization of an RNA-mimic substrate, uridine-3′-2,2,2-chloroethyl phosphate (**2**), in aqueous solution at pH 7.0, with rate enhancements more than 2 orders of magnitude larger than the imidazole catalyzed reaction (k_2(Pep)/k_2(Im) = 252). The reactivity achieved with this 42-residue polypeptide is based on two histidine and four arginine residues located on the surface of each helix−loop−helix motif, and it is probably due to a combination of nucleophilic and general acid−base catalysis, as suggested by the pH dependence and the observed kinetic solvent isotope effect, together delivering effective transition state stabilization. Consequently, an improved combination of structural stability, charge distribution and equilibration, hydrophobic core interactions, and catalytic residues has been achieved in this peptidic scaffold. The observed rate enhancements are of the same order of magnitude as those found with more reactive substrates, making catalysts for **2** good models for catalysts ultimately expected to catalyze RNA. The results therefore represent an important step forward in the design of catalysts for RNA cleavage and set the stage for the further development of a *de novo* engineered artificial ribonuclease, since the catalyst could readily be linked to PNA in order to add the required sequence recognition to the cleaving activity. Once again, the usefulness and potential of the helix−loop−helix motif as a scaffold to engineer and accommodate many different functions have been demonstrated.

Experimental Section

Instruments and General Methods. ^{1}H, ^{13}C, and ^{31}P NMR spectra were obtained in D_2O, H_2O/D_2O 90/10, or $CDCl_3$ solutions on a Varian Mercury 300 or Varian Inova Unity 600 MHz. MALDI-TOF mass

(30) Laughton, P. M.; Robertson, R. E. In *Solute-Solvent Interactions*; Coetzee, J. F., Ritchie, C. D., Eds.; Marcel Dekker: New York, 1969; pp 399−525.
(31) Li, N. C.; Tang, P.; Mathur, R. *J. Phys. Chem.* **1961**, *65*, 1074−1076.
(32) (a) Frey, P. A.; Hegeman, A. D. In *Enzymatic Reaction Mechanisms*; Oxford University Press: 2007; p 541. (b) Marnett, E. M.; McKelvey, D. R. In *Enzymatic Reaction Mechanisms*; Oxford University Press: 2007; pp 343−398. (c) Kresge, A. J.; More O'Ferral, R. A.; Powell, M. F. In *Isotopes in Organic Chemistry*; Buncel, E., Lee, C. C., Eds.; Secondary and Solvent Isotope Effects; Elsevier: Amsterdam, 1987; Vol. 7, pp 177−273. (d) Kirby, A. J.; Younas, M. *J. Chem. Soc. B* **1970**, 1165−1172. (e) Anslyn, E.; Breslow, R. *J. Am. Chem. Soc.* **1989**, *111*, 8931−8932.

spectrometry was performed on an Applied Biosystems Voyager DE-STR mass spectrometer in a 1:10 sample/matrix relation, using α-cyano-4-hydroxycinnamic acid as a matrix. All the water solutions were prepared from distilled and filtered water.

Preparation of Substrates. See Supporting Information (pages S1−S4).

Kinetics. The kinetic measurements were obtained from experiments performed in parallel using samples prepared from the same substrate, imidazole, or peptide stock solutions to avoid interexperimental errors. They were run in buffered solutions using 50 mM sodium actetate in the 4.3−5.0 pH range, 50 mM MES from pH 5.2 to pH 6.5, and 50 mM HEPES for kinetics between pH 7.0 and 8.0. NaCl was added to obtain the same final salt concentration and maintain a constant ionic strength in all experiments. The reaction temperature was controlled by a thermostatic bath where the tightly stoppered reaction vessels were kept. Peptide samples were prepared as a stock solution by dissolving the lyophilized peptide in the reaction solvent, adjusting the pH, and centrifuging prior to being diluted by pipetting to the desired concentrations and transferred to the reaction vessel. In the same way, imidazole and substrates were weighed and dissolved in the reaction solvent, the pH was adjusted, and the required volume was taken from the stock solutions. The measurements started after fast mixing of the reactants, shaking of the vessels, and reintroduction in the thermostated bath, and the evolution of the reaction was followed by the periodical quantification of product formation by way of NMR or HPLC analysis. For rate constant calculations, the experimental data points of product concentration were plotted against time, the points were adjusted to lines by linear regression, and the rates were calculated from the values of the slopes using Igor Pro software (Wavemetrics Inc.). To obtain the second-order rate constants, k_2, the background reaction was substracted from the measured pseudo-first-order rates and divided by the initial concentration of the catalyst and substrate.

NMR Kinetic Experiments. The experiments were run in a 600 MHz spectrometer (Varian Inova Unity 600 MHz) at three diferent pH values: 5.0, 6.0, and 7.0 using 50 mM buffers. At each pH value, three samples in tightly stoppered NMR tubes were used: peptide (HNI 3 mM), imidazole (100 mM), and the blank experiment (background reaction) with final volumes of 0.6 mL with the same concentration of substrate (30 mM) and salt (100 mM NaCl). Solvents used were D_2O or H_2O/D_2O 90/10 v/v and temperature controlled by a thermostatic bath at 323 K while tubes were periodically shaken. The evolution of the reaction was followed by measuring the increase of the NMR signal of the methyl group from the formed cyclization product, propane-1,2-diol cyclic phosphate (doublet at δ 1.28 ppm). Since the reaction is very slow and only a very small amount of product is formed (less than 14% in the fastest run, at pH 7.0, after 391 days), the ^{13}C satellite signal of the initial substrate was used as an internal reference and the product concentrations were calculated from the comparison of integration values. The pulse sequence was optimized to ensure that enough time was allowed for relaxation between pulses to get the best signal-to-noise ratios for selected signals from substrate and product.

HPLC Kinetic Experiments. Reactions were carried out in tightly stoppered glass bottles with a final volume of 0.6 mL. Ten different pH values were checked: 4.3, 4.5, 4.8, 5.0, 5.2, 5.6, 6.0, 6.5, 7.0, and 8.0. At each pH value, three samples were prepared: peptide (HNI 1 mM), imidazole (50 mM), and the blank experiment (background reaction) with the same concentration of substrate (2 mM), salt (50 mM NaCl), and internal standard (3-nitrobenzenesulfonic acid, sodium salt, 1 mM). The experiments were run in H_2O or D_2O using 50 mM buffers at 313 K (temperature controlled by a thermostatic bath), and bottles were periodically shaken. The reaction rates were determined by RP-HPLC, measuring the concentration increase of the hydrolysis product, uridine 2′,3′-cyclic phosphate, with the detector at 260 nm. Aliquots were withdrawn at suitable intervals and analyzed immediately or kept frozen (liquid nitrogen). Column: Highchrom KR-100-C8-5 (250 mm × 4.6 mm, 5 μm particle size). Isocratic elution with 13% acetonitrile in sodium acetate buffer (25 mM, pH 4.3, containing 0.1 M NH_4Cl) as eluent in a 1.5 mL/min flux. Retention times of product, internal standard, and substrate were 1.89, 5.66, and 8.62 min, respectively.

Saturation Kinetics. The saturation experiments were run at pH 7.0 (50 mM HEPES buffer) and 313 K, preparing the samples to have the same concentration of peptide (HNI 0.5 mM) and internal standard (3-nitrobenzenesulfonic acid, sodium salt, 2 mM). Then, six different experiments were performed with increasing amounts of substrate, 5, 10, 20, 25, 30, and 40 mM, and decreasing amounts of salt (NaCl) added to equilibrate ionic strength. A parallel experiment is run to check the background reaction (blank). The evolution of the reaction is followed by RP-HPLC, in the same way shown before.

Peptide Synthesis. The peptide was synthesized on an automated peptide synthesizer (Pioneer, Applied Biosystems) at a 0.1 mmol scale with a standard Fmoc (9-fluorenylmethoxycarbonyl protection group) protocol. The Fmoc protecting group was removed by 20% piperidine in DMF v/v. A 0.19 mmol g^{-1} substitution level polymer (PAL-PEG-PS) was used, with an excess of 4 equiv of amino acid in each coupling, base-stable protecting groups for side chain protection, and TBTU (0.5 M in DMF) and DIPEA (1 M in DMF) as amino acids activators. Standard coupling times were 60 min, except for Nle and Leu (30 min) and for Gln, Arg, and Asn (90 min). The amino terminal was capped with acetic acid anhydride and carboxy terminal amidated upon cleavage from the resin. When synthesis was complete, the resin was washed with dichloromethane and dried under vacuum. The peptide was then cleaved from the resin and deprotected at room temperature by treatment with a mixture of TFA/H_2O/ethanedithiol/triisopropyl silane (94:2.5:2.5:1 v/v) for 3 h. It was then filtrated, concentrated (N_2 bubling), precipitated by addition of cold diethyl ether, washed with diethyl ether, centrifuged, and lyophilized two times. The purification of crude peptide was accomplished by reversed phase HPLC on a semipreparative column (C-8 Kromasil) using isocratic elution with 37% 2-propanol in water with 0.1% TFA at a 10 mL/min flow rate. The peptide was identified by MALDI-TOF mass spectrometry (Applied Biosystems), and no impurities could be detected by HPLC (detector at 229 nm).

Acknowledgment. The authors wish to thank A. J. Kirby for his many insightful comments and contributions and his help with the manuscript and also the rest of ENDEVAN (European Network on the Development of Artificial Nucleases) members for interesting discussions, especially R. Stromberg for useful suggestions about the uridine derivative and initial sample. J.R. was supported by the European Commission under the Human Potential Programme (ENDEVAN, HPRN-CT-1999-00008), and financial support was also obtained from the EC, which is gratefully acknowledged.

Supporting Information Available: Preparation of substrates. Figure S1: Complete kinetic profile for the cyclization of substrate **2** at pH 7.0 and 313 K. Figure S2: Catalysis of the reaction of substrate **2** by HNI as a function of substrate concentration in the range from 5 to 40 mM. Figure S3: Representative HPLC chromatogram of substrate **2** kinetics. Figure S4: Representative ^1H NMR spectrum of substrate **3** kinetics. Figure S5: ^1H NMR spectra of substrates **2** and **3** and intermediate phosphates. This material is available free of charge via the Internet at http://pubs.acs.org.

JA075478I